ANNALS of Clinical and Translational Neurology
Open Access
AMERICAN NEUROLOGICAL ASSOCIATION
INNOVATORS IN DISCOVERY, EDUCATION, AND CARE

RESEARCH ARTICLE

Clinical relevance of paramagnetic rim lesion heterogeneity in multiple sclerosis

Anna Stölting[1], Colin Vanden Bulcke[1,2], Serena Borrelli[1,3], Céline Bugli[4], Renaud Du Pasquier[5], Vincent van Pesch[6] & Pietro Maggi[1,6]

[1]Neuroinflammation Imaging Lab (NIL), Institute of NeuroScience, Université catholique de Louvain, Brussels, Belgium
[2]ICTEAM Institute, Université catholique de Louvain, Louvain-la-Neuve, Belgium
[3]Department of Neurology, Hôpital Erasme, Hôpital Universitaire de Bruxelles, Université Libre de Brussels, Brussels, Belgium
[4]Plateforme technologique de Support en Méthodologie et Calcul Statistique, Université catholique de Louvain, Brussels, Belgium
[5]Neurology Service, Department of Clinical Neurosciences, University Hospital of Lausanne and University of Lausanne, Lausanne, Switzerland
[6]Department of Neurology, Cliniques universitaires Saint-Luc, Université catholique de Louvain, Brussels, Belgium

Correspondence
Pietro Maggi, Cliniques Universitaires Saint-Luc, Av. Hippocrate 10, Brussels 1200, Belgium. Tel: +32 27641111; E-mail: pietro.maggi@uclouvain.be

Received: 2 September 2024; Revised: 24 September 2024; Accepted: 14 September 2024

***Annals of Clinical and Translational Neurology* 2024; 11(12): 3137–3151**

doi: 10.1002/acn3.52220

Abstract

Objective: Previous studies reveal heterogeneity in terms of paramagnetic rim lesions (PRL) associated tissue damage. We investigated the physiopathology and clinical implications of this heterogeneity. **Methods**: In 103 MS patients (72 relapsing and 31 progressive), brain lesions were manually segmented on 3T 3D-FLAIR and rim visibility was assessed with a visual confidence level score (VCLS) on 3D-EPI phase. Using T1 relaxation time maps, lesions were categorized in long-T1 and short-T1. Lesion age was calculated from time of first gadolinium enhancement (N = 84 lesions). Results on clinical scores were validated in an extended cohort of 167 patients using normalized T1w-MPRAGE lesion values. **Results**: Rim visibility (VCLS analysis) was associated with increasing lesional T1 ($P/P_{FDR} < 0.001$). Of 1680 analyzed lesions, 427 were categorized as PRL. Long-T1 PRL were older than short-T1 PRL (average 0.8 vs. 2.0 years, P/P_{FDR} = 0.005/0.008), and featured larger lesional volume ($P/P_{FDR} < 0.0001$) and multi-shell diffusion-measured axonal damage ($P/P_{FDR} < 0.0001$). The total volume of long-T1-PRL versus PRL showed 2× predictive power for both higher MS disability (EDSS; P/P_{FDR} = 0.003/0.005 vs. P/P_{FDR} = 0.042/0.057) and severity (MSSS; P/P_{FDR} = 0.0006/0.001 vs. P/P_{FDR} = 0.004/0.007). In random forest, having ≥1 long-T1-PRL versus ≥4 PRL showed 2-4× higher performance to predict a higher EDSS and MSSS. In the validation cohort, long-T1 PRL outperformed (~2×) PRL in predicting both EDSS and MSSS. **Interpretation**: PRL show substantial heterogeneity in terms of intralesional tissue damage. More destructive, likely older, long-T1 PRL improve the association with MS clinical scales. This PRL heterogeneity characterization was replicated using standard T1w MRI, highlighting its potential for clinical translation.

Introduction

Since the earliest stages of multiple sclerosis (MS), smoldering inflammation has emerged as a major driver of disability accumulation independent of relapse activity.[1,2] In this context, focal smoldering/chronic active MS lesions (CAL) are associated with disease severity and progression.[3–5]

On histopathology, CAL are heterogeneous in terms of inflammatory cells' proportion and distribution (i.e., rim thickness);[6,7] however, whether this relates to the temporal development and evolution of CAL in living MS patients is hard to ascertain from autopsy studies. Brain magnetic resonance imaging (MRI) represents a unique opportunity to study the development of MS lesions *in vivo*. Susceptibility-based MRI techniques can depict a subset of CAL featuring a perilesional inflammatory rim of iron-laden microglia and macrophages.[8] These paramagnetic rim lesions (PRL) are more destructive than other MS lesions types,[9–11] feature an impaired lesional

and peri-lesional tissue microstructure,[12–14] longer T1 relaxation times[15,16] and larger volumes.[11] PRL can be found in both relapsing–remitting and progressive MS.[3,5,9,12,16]

In agreement with postmortem histopathology,[6] recent quantitative MRI studies have shown heterogeneity in terms of PRL-associated tissue damage.[12,16] Existing MRI evidence on the temporal development of CAL suggests dynamic changes in lesional volume,[3,9–11] apparent diffusion coefficient,[18] magnetic susceptibility,[19] and T1 intensity values during the early development of these lesions.[11] However, the clinical significance of these changes is still largely unknown. Interestingly, thresholding MS lesions based on their T1 relaxation times seems to improve the correlation with clinical scores.[20]

With this background, we address two critical questions regarding the physiopathology of CAL and their clinical significance: (1) how does the MRI-measured tissue damage evolve within PRL over time? and (2) can this MRI-based tissue damage characterization improve our prediction of clinical outcomes? By marshaling both advanced and more established MRI techniques such as quantitative T1 mapping, diffusion MRI, and semiquantitative T1w images, we studied the heterogeneity of PRL-associated tissue damage and its importance in predicting clinical outcomes in a multicentric cohort of MS patients.

Material and Methods

Study participants

Clinical and imaging data were collected under institutional review board-approved protocols in two university hospitals (Cliniques universitaires Saint-Luc, Brussels, Belgium, and Centre Hospitalier Universitaire Vaudois, Lausanne, Switzerland). These protocols allowed exploratory analysis and pooling of collected data. Clinical information including MS disability (expanded disability status scale (EDSS))[21] and severity (multiple sclerosis severity scale (MSSS))[22] scales were obtained from experienced MS clinicians at the time of each MRI scan. Clinico-radiological relapse was defined as the presence of newly appearing or contrast-enhancing MRI lesions and/or new neurological symptoms in the 3 months preceding the baseline assessment.

Patient inclusion criteria encompassed (1) age ≥18 years, (2) diagnosis of relapsing–remitting MS (RRMS), secondary progressive MS (SPMS), or primary progressive MS (PPMS) according to the 2017 McDonald MS Criteria,[23] availability of (3) a 3-Tesla (3T) high-resolution susceptibility-based MRI and of a T1-weighted magnetization prepared rapid gradient echo images (MPRAGE), and (4) of a matched clinical-MRI assessment at baseline. Participants who underwent MRI in Brussels also had an available quantitative T1 map (see below MRI acquisition and analysis). Thus, all included patients had susceptibility-based MRI and MPRAGE – hereafter, "MPRAGE cohort", whereas only participants in Brussels had available T1 mapping – hereafter, "T1 mapping cohort".

For the participants of the T1 mapping cohort, whenever available, additional prospectively yearly acquired follow-up MRI scans were included in the analysis. Furthermore, and only for the participants who underwent MRI in Brussels, retrospective analysis of archival 1.5 or 3T MRI scans were reviewed for the presence of lesional gadolinium enhancement. Please note that these archival 1.5 or 3T MRI scans were used exclusively to calculate lesion age (see "Lesion age analysis" below). They were not used for assessing lesional paramagnetic rim visibility or for MP2RAGE/MPRAGE-based analyses (see "MRI acquisition and analysis" below).

All participants provided written informed consent prior to the study.

MRI acquisition and analysis

MRI studies were performed on a 3T SIGNA™ scanner (GE Health Care) in Brussels, Belgium or a 3T Magnetom Skyra or Prisma-fit scanner (Siemens Healthcare) in Lausanne, Switzerland. The imaging protocol in both centers included a 3T high-resolution 3D T2* echoplanar imaging (EPI) sequence for PRL detection, a fluid-attenuated inversion recovery (FLAIR) sequence for lesion segmentation and a T1-weighted image acquired post intravenous injection of a single dose (0.1 mmol/kg) of gadobutrol ((gad), Gadavist; Bayer Healthcare, Leverkusen, Germany) to detect acute inflammation. Brain lesions were further stratified based on their 3D magnetization-prepared two rapid gradient echo (MP2RAGE) derived T1 times (available for Brussels participants only – T1 mapping cohort) and their MPRAGE derived T1 normalized intensity values (available for all included patients – MPRAGE cohort).

Participants of the T1 mapping cohort also had an additional multi-shell diffusion-weighted sequence to estimate tissue integrity. Brain volumes were computed using FreeSurfer on MPRAGE images.[24]

Additional MRI methods are detailed in Data S1.

PRL assessment

For each participant, the presence of PRL on unwrapped phase images was independently assessed by two raters (A.S. and P.M.). In case of initial disagreement,

agreement was reached in a separate session by consensus between the two raters. PRL were assessed following the North American Imaging in Multiple Sclerosis (NAIMS) guidelines.[25]

Paramagnetic rim visibility analysis

On a subset of participants consecutively drawn from the T1 mapping cohort, after initial PRL assessment, rim visibility on phase images was assessed using a 5-point Likert visual confidence level score (VCLS) as followed (Fig. 2):

- Confidence level 1 – **No paramagnetic rim**
- Confidence level 2 – **Doubtful**
- Confidence level 3 – **Neutral**
- Confidence level 4 – **Certain**
- Confidence level 5 – **Very certain paramagnetic rim**

Initial VCLS assessment was performed by A.S. In order to estimate respectively the inter-rater and intra-rater reliability, a subset of 70 randomly selected lesions was independently assessed by P.M. and a randomly selected dataset of 380 lesions was reassessed by A.S. after 6 months. In-depth overview of the VCLS criteria can be found in Data S1.

Lesion volumetric and microstructural analysis

Independently of their VCLS rating, all lesions were then manually segmented on coregistered FLAIR images using ITK-SNAP (www.itksnap.org). Baseline segmentations were manually/visually adapted to match lesion's size changes over the MRI follow-up. Microstructural lesion tissue integrity was investigated using two quantitative and one semiquantitative imaging method: (i) quantitative MP2RAGE-derived T1-maps, which have previously been shown to be an established marker of MS tissue integrity,[15] (ii) multi-shell diffusion MRI, using neurite orientation dispersion and density imaging (NODDI),[26] and (iii) normal appearing white matter (NAWM) normalized MPRAGE images. Lesional mean T1 time, mean normalized MPRAGE intensity value, diffusion metrics (including Neurite Density Index (NDI) and extraxonal cell volume fraction (ECVF)), and volume were calculated.

Lesion age analysis

Only for participants who underwent MRI in Brussels (T1 mapping cohort) and for which longitudinal and/or retrospective (see below) MRI scans were available for review, analysis of lesion age was performed. Each lesion was initially checked for gad enhancement on available MRI scans also including, whenever accessible, archival longitudinal 1.5 or 3T MRI scans patients had received before inclusion in the present study. Lesion age was calculated as the time interval between initial gad enhancement and the time of a specific MRI scan. Moreover, if new lesions appeared between two MRI scans, the lesion age was estimated as half the time elapsed between the two scans. Of note, lesions that showed gad enhancement within the last 6 months were excluded from further analysis to eliminate any possible influence of acute inflammatory activity.[25]

Lesion categories based on qualitative and quantitative analysis

The "long-T1" cutoff was calculated based on the T1 relaxation times (or normalized T1 MPRAGE intensity values) distribution (75th percentile), grounded on the whole lesion population, after exclusion of gad-enhancing lesions – see also below, "Statistical analysis". Based on this quantitative (or semiquantitative) approach, lesions were classified into two groups: "long-T1" and "short-T1" lesions. In order to compare this quantitative approach with a previously proposed histopathologically validated qualitative one,[15] a subset of 50 randomly selected lesions were visually rated by A.S. based on their MP2RAGE T1 maps and T1-weighted MPRAGE intensities. Inter-rater reliability was assessed in a subset of 30 randomly chosen lesions independently rated by P.M. Based on this visual assessment lesions were classified in three groups, as previously described:[15] "short-T1 lesions" are isointense to the cortex, "long-T1 lesions" are clearly hyperintense to the cortex (and nearly isointense to CSF) on T1 maps and showed "black holes" on MPRAGE, and "mixed-lesions" showed intermediate signal intensity or well-defined areas of high/low signal intensity.[15] Finally the agreement between qualitative method (three groups) and the quantitative one (two groups) was tested after merging visually rated short- and mixed-T1 lesions.

Statistical analysis

Statistical analysis was performed using R[27] and SPSS (IBM SPSS Statistics for Windows, Version 29.0.1.0).

The main hypothesis of this study was that characterizing PRL heterogeneity could improve their association with clinical outcomes. To verify this hypothesis, we investigated the PRL heterogeneity with respect to lesional rim visibility and lesional age (see here below, "Lesion-based analysis"). Then, we tested whether the observed PRL heterogeneity could improve the associations with clinical scores (see below, "Clinical analysis").

Lesion-based analysis

To avoid outliers coming from quantitative T1 estimation in uncommonly large and confluent lesions, lesions were thresholded based on the 95th percentile lesion volume cutoff (calculated in non-active lesions). To compare the lesional tissue integrity assessment obtained with quantitative T1 mapping versus semiquantitative normalized MPRAGE, Pearson correlation, and linear regression analysis were used. The association between mean lesional T1 times, normalized T1 intensities or lesional volumes (dependent variables) with rim visibility (VCLS scale) was tested in three distinct mixed models with random subject effect. The VCLS was considered as a fixed effect variable. The inter-rater agreement (two raters) for the PRL assessment (PRL vs. non-PRL) was computed using Cohen κ, while the VCLS and qualitative intensity rating (ordinal variables) were computed using weighted Cohens κ.

Mixed models with random subject effect were used to model (1) lesional T1 in PRL and non-PRL and (2) VCLS, in relation to patients' age. The behavior of lesional T1 within short-T1 and long-T1 PRL over time was modeled using a repeated measures mixed model with random subject and random lesion effect. Estimate β_{add} indicates the difference in T1 change over time.

Clinical analysis

Patients were categorized according to the number of PRL, long-T1 PRL and short-T1 PRL, based on the distribution of the data in this study (and using the 75th percentile as a cutoff). In a second analysis, patients were recategorized in either having 0 PRL, only short-T1 PRL, or at least one long-T1 PRL. Additionally, the clinical associations were also explored as a function of the total lesion volume/patient of PRL, long-T1 PRL, and short-T1 PRL.

Baseline differences (demographic and clinical) between patient groups were assessed in univariable analysis using t-test, Mann–Whitney *U*-test, or chi-squared tests, as appropriate.

Univariate linear models were used to test the association between the clinical disability and severity scales (EDSS and MSSS, dependent variable) and the different PRL, long-T1 PRL, and short-T1 PRL categories. Random forest analysis (R – random forest)[28] was used to specify predictive value of each variable, splitting data in training and testing subsets (70% and 30%), ensuring balanced distribution of center and dependent variable between subsets. Each model was implemented using 500 trees and best mtry (i.e., the number of variables to randomly sample as candidate at each split) was chosen based on model strength. Variable importance was ranked by assessing mean decrease accuracy (MDA), computed from out-of-bag data permutation, and percent increase in mean squared error (%IncMSE). Benjamini–Hochberg procedure was used to calculate the false discovery rate (FDR) and adjusted *P*-values. Uncorrected (P) and corrected (P_{FDR}) *P*-values are reported for all results.

Results

Of the total 167 patients included in the study, 103 patients (72 RRMS and 31 progressive MS (PMS)(21 SPMS and 10 PPMS)) belonged to the T1 mapping cohort (Fig. 1). Of these 103 patients, 53 had a first-year and 15 also a second-year MRI follow-up scan. The median time between baseline, first, and second follow-up MRI was respectively 12.8 (range: 8–16) and 25.8 (range: 12–34) months. In all patients of the T1 mapping cohort, a total of 2281 lesions were manually segmented and analyzed at baseline. To avoid outliers coming from uncommonly large and confluent lesions (see above, Statistical analysis), 117 lesions were excluded from further analysis (95th percentile lesional volume cutoff = 423 mm^3).

Lesional paramagnetic rim visibility using VCLS

Of the total 2281 lesions segmented at baseline, the visibility of the paramagnetic rim was rated in 1680 lesions coming from a subset of 88 patients consecutively included in the T1 mapping cohort. Of these 1680 lesions, 1253 were rated confidence levels 1–3 ("no paramagnetic rim": 483 (28.75%); "doubtful," 348 (22.86%) and "neutral," 422 (25.12%)), while 427 lesions were rated either "certain" PRL (237, 14.11%) or "very certain" PRL (190, 11.31%). Considering certain and very certain lesions as PRL, 237 out of 427 (55.56%) were VCLS 4 and 190 out of 427 (44%) were VCLS 5. Inter-rater agreement was substantial (weighted Cohens $\kappa = 0.74$, $P/P_{FDR} < 0.0001$). Intra-rater agreement was almost perfect (weighted Cohens $\kappa = 0.932$, $P/P_{FDR} < 0.0001$).

The linear mixed model with random subject effect showed that lesional T1 times significantly differed between all visual confidence levels (besides VCLS 2 and 3 where no significant difference was found; $P/P_{FDR} = 0.93/0.99$) and that longer lesional T1 times were associated with better rim visibility (Fig. 2). Other differences in MRI metrics between VCLS lesions are reported in Table S1. Similar results were obtained when using the more clinically available MPRAGE sequence (Data S1 and Table S1).

Modeling of lesion VCLS over patient age found a significant time effect with decreasing rim visibility over

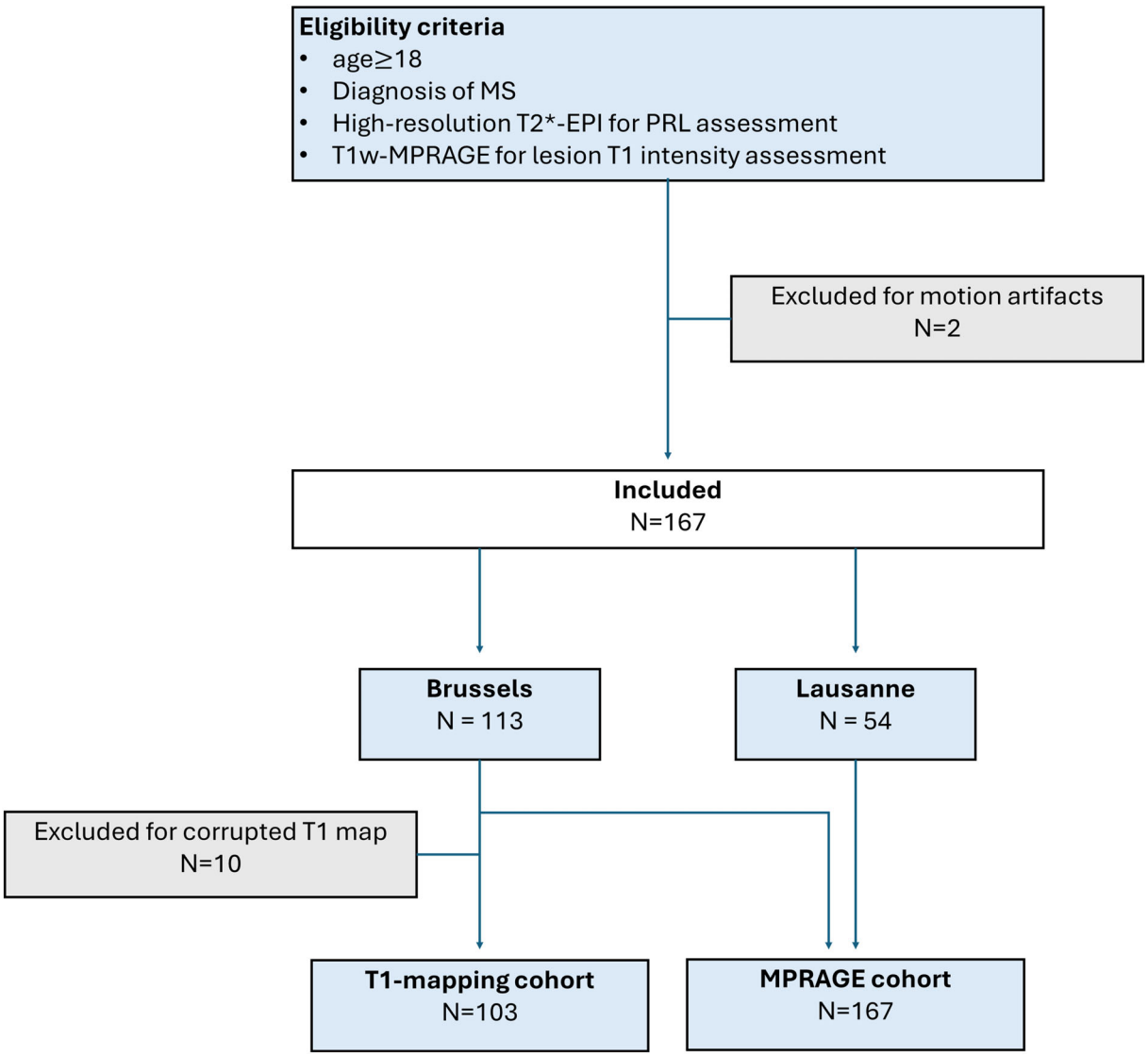

Figure 1. Flowchart summarizing patients' inclusion into the study. T2*-EPI, submillimeter isotropic 3D T2*-weighted segmented echo planar imaging; MPRAGE, magnetization prepared rapid gradient echo.

patient age (β = −0.02/year, 95% CI [−0.03 to −0.1], $P/P_{FDR} < 0.001$), suggesting that paramagnetic rims are less prominent in older patients. Interestingly, our exploratory analysis in the small sample of lesions for which age tracking was available ($N = 84$) did not show any difference in terms of lesion age between VCLS 4 and VCLS 5 (P/P_{FDR} = 0.26/0.31).

For subsequent analyses, certain and very certain PRL (VCLS 4 and 5) were denoted as "PRL", whereas VCLS 1–3 lesions were denoted as "non-PRL". Inter-rater agreement for PRL status was substantial (Cohens κ = 0.738, $P/P_{FDR} < 0.0001$) while intra-rater agreement was almost perfect (Cohens κ = 0.928, $P/P_{FDR} < 0.0001$).

Observed baseline differences between PRL and non-PRL are in line with previous studies[10–13] and are reported in Data S1.

Heterogeneity in PRL-associated tissue damage

A substantial lesional T1 heterogeneity was observed in PRL and non-PRL (Fig. 3A). Modeling of average lesional T1 over the patient age and PRL status found that PRL (vs. non-PRL) showed a significantly accelerated T1 time increase over time (β_{add} = 4.16 ms/year, 95% CI [1.73–6.5] P/P_{FDR} = 0.0008/0.002; Figure S3).

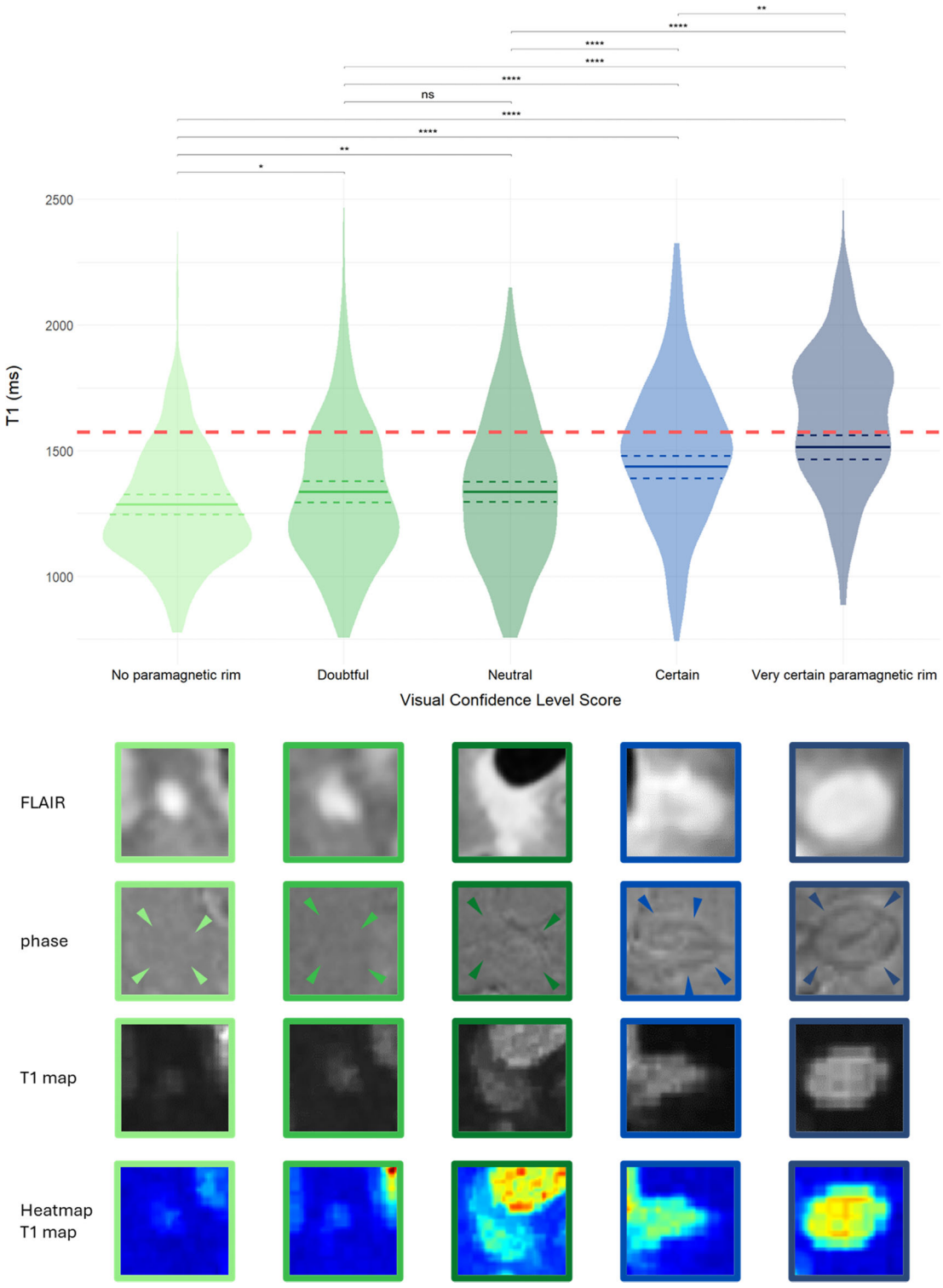

Figure 2. Visual Confidence Level Score (VCLS) and the relationship with T1. Significantly increased T1 values with rising VCLS. Solid line indicates calculated estimate after repeated measure mixed model analysis, dashed line indicates 95% confidence interval. Red dashed line shows long-T1 cutoff at 1572 ms. VCLS 1 = "no paramagnetic rim," VCLS 2 = "doubtful," VCLS 3 = "neutral," VCLS 4 = "certain," VCLS 5 = "very certain paramagnetic rim"; ns = not significant, *$P/P_{FDR} < 0.05$, **$P/P_{FDR} < 0.01$, ***$P/P_{FDR} < 0.001$, ****$P/P_{FDR} < 0.0001$.

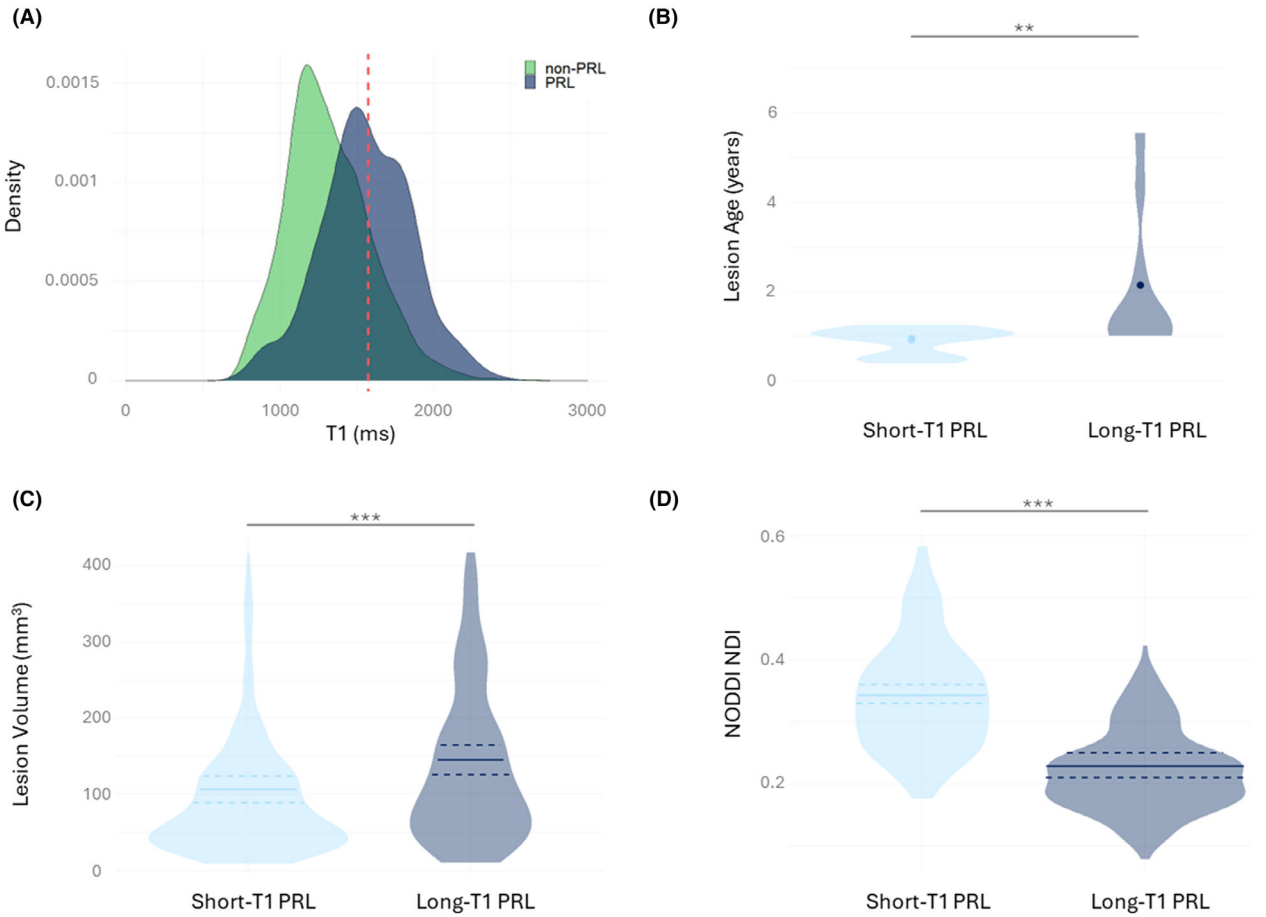

Figure 3. PRL heterogeneity and its importance in lesion stratification. (A) Density plot of T1 values in non-PRL and PRL. Red line indicates calculated long-T1 cutoff at 1572 ms. $N = 1860$. (B) Lesion age comparison between short-T1 and long-T1 PRL. $N = 39$. (C) Lesion volume comparison between short-T1 and long-T1 PRL. $N = 427$. (D) NODDIs NDI comparison between short-T1 and long-T1 PRL. $N = 427$. ns = not significant, $*P/P_{FDR} < 0.05$, $**P/P_{FDR} < 0.01$, $***P/P_{FDR} < 0.001$, $****P/P_{FDR} < 0.0001$. NDI, Neurite Density Index; NODD, neurite orientation dispersion and density imaging.

On the whole lesion cohort (PRL and non-PRL), the long-T1 relaxation time cutoff (75th percentile) to differentiate short-T1 and long-T1 lesions was estimated at 1572 ms. Similarly, we calculated a normalized MPRAGE intensity value cutoff at −3.31 SD. Cohen κ for the agreement between long-T1 cutoffs using T1 mapping versus MPRAGE was at 0.67 ($P/P_{FDR} < 0.0001$; Figure S1). Out of 427 PRL analyzed in the T1 mapping cohort, 196 PRL (45.9%) surpassed the long-T1 cutoff (hereafter "long-T1 PRL"), while 231 did not (hereafter "short-T1 PRL").

A subset of 50 randomly chosen lesions were qualitatively rated based on their T1 map intensity, as previously described.[15] The initial agreement between raters was moderate (weighted Cohens $\kappa = 0.572$, $P/P_{FDR} = 0.004/0.006$); discrepancies were discussed, and a final agreement was reached. Fifteen lesions (30%) were rated as short-T1, 19 (38%) as mixed-T1 and 16 (32%) as long-T1 lesions. Using the quantitative T1 relaxation time cutoff from the original lesion cohort, 17 out of the 50 visually rated lesions (34%) surpassed the long-T1 cutoff. The agreement between qualitative and quantitative methods was strong (Cohens $\kappa = 0.864$, $P/P_{FDR} < 0.0001$; Figure S4).

Long-T1 PRL (vs. short-T1 PRL) showed significantly larger lesion volume (mean 145.01 vs. 106.14 mm^3, $P/P_{FDR} < 0.0001$), reduced NDI (mean 0.23 vs. 0.34, $P/P_{FDR} < 0.0001$), and higher ECVF (mean 0.59 vs. 0.54, $P/P_{FDR} < 0.0001$). In this PRL lesion cohort, the median follow-up duration (scans with available T1 mapping) was 391 days (range: 274–931 days). When modeling average lesional T1 over follow-up duration, short-T1 PRL (vs. long-T1 PRL) showed increasing T1 values over time ($\beta_{add} = 43.97$ ms/year, 95% CI [17.537–70.407], $P/P_{FDR} = 0.001/0.002$; Figure S5).

Table 1. Clinical and MRI demographics of the T1 mapping cohort.

	Long-T1 PRL categorization			Classical PRL categorization		
Characteristic	0 long-T1 PRL $N = 66$[a]	≥1 long-T1 PRL $N = 37$[a]	P/P_{FDR}[b]	0–3 PRL $N = 75$[a]	≥4 PRL $N = 28$[a]	P/P_{FDR}[b]
Age	43.43 (13.09)	46.15 (13.06)	0.3/0.4	46.03 (13.57)	40.06 (10.73)	**0.042/** 0.057
Sex						
Male	20/66 (30%)	16/37 (43%)	0.2/0.3	25/75 (33%)	11/28 (39%)	0.6/0.6
Female	46/66 (70%)	21/37 (57%)		50/75 (67%)	17/28 (61%)	
Phenotype						
RRMS	52/66 (79%)	20/37 (54%)	**0.009/0.014**	54/75 (72%)	18/28 (64%)	0.4/0.4
PMS	14/66 (21%)	17/37 (46%)		21/75 (28%)	10/28 (36%)	
Disease duration	8.87 (9.45)	9.16 (10.23)	0.7/0.7	10.06 (10.24)	6.06 (7.43)	0.051/ 0.069
Treatment at baseline						
Untreated	35/66 (53%)	22/37 (59%)	0.4/0.4	46/75 (61%)	11/28 (39%)	0.2/0.2
Platform	4/66 (6.1%)	1/37 (2.7%)		4/75 (5.3%)	1/28 (3.6%)	
High efficacy	20/66 (30%)	7/37 (19%)		17/75 (23%)	10/28 (36%)	
Very high efficacy	7/66 (11%)	7/37 (19%)		8/75 (11%)	6/28 (21%)	
EDSS	2.39 (1.82)	3.72 (2.22)	**0.010/0.015**	2.72 (2.02)	3.27 (2.15)	0.4/0.5
MSSS	3.96 (2.44)	5.80 (2.38)	**<0.001/ <0.001**	4.25 (2.48)	5.63 (2.55)	**0.020/ 0.028**
Norm. brain volume	0.74 (0.03)	0.73 (0.03)	0.2/0.2	0.74 (0.03)	0.75 (0.03)	0.11/0.14
Norm. thalamic volume	0.0088 (0.00097)	0.0084 (0.00082)	**0.014/0.02**	0.0087 (0.00097)	0.0086 (0.0089)	0.5/0.5
Norm. CP volume	0.0016 (0.0003)	0.0018 (0.0003)	**0.009/0.014**	0.0017 (0.0003)	0.0018 (0.0003)	0.2/0.2
T2 lesion load	5,822.55 (6,485.61)	10,234.78 (9,001.95)	**0.001/0.002**	6,869.01 (7,605.92)	8,849.96 (8,055.39)	0.10/0.13
Number of cortical lesions	6.17 (8.66)	15.38 (29.15)	**0.008/0.012**	7.37 (11.85)	15.11 (30.95)	0.064/ 0.085

Treatments: platform = injectable platform drugs; high efficacy = teriflunomide, dimethyl fumarate, fingolimod, siponimod, and ozanimod; very high efficacy = ocrelizumab, ofatumumab, rituximab, natalizumab, and cyclophosphamide. Bold *P*-values indicate statistical significance ($P < 0.05$). CP, choroid plexus; EDSS, Expanded Disability Status Scale; MS, multiple sclerosis; MSSS, Multiple Sclerosis Severity Score; lT1-PRL, long-T1 paramagnetic rim lesion; PMS, primary or secondary progressive MS; PRL, paramagnetic rim lesion; RRMS, relapsing–remitting MS; normalized volumes = total structure volume/intracranial volume.

[a]Mean (SD); *n*/*N* (%).

[b]Wilcoxon rank sum test; Pearson's chi-squared test; Fisher's exact test.

Finally, our exploratory analysis on the small sample of age-tracked PRL ($N = 39$) showed that long-T1 PRL ($N = 10$, 25.6%) were older than short-T1 PRL ($N = 29$, 74.4%; mean 2.0 vs. 0.8 years, $P/P_{FDR} = 0.005/0.008$). Age-tracked non-PRL ($N = 45$) did not show any age differences between short-T1 and long-T1 non-PRL ($P/P_{FDR} = 0.66/0.71$).

Clinical associations in the T1 mapping cohort

Of the 103 patients included in the T1 mapping cohort, 61 (59.2%) had at least one PRL. There was no difference in the number of PRL ($P/P_{FDR} = 0.49/0.53$) or number of short-T1 PRL ($P/P_{FDR} = 0.26/0.33$) between disease phenotypes. Instead, the number of long-T1 PRL was higher in PMS versus RRMS patients (median: 1, range: 0–15 vs. median 0, range: 0–48, $P/P_{FDR} = 0.008/0.01$). Roughly 27% of RRMS patients and 54% of PMS patients had at least one long-T1 PRL (Table 1). Baseline correlations of different MRI lesion metrics, including total PRL, short-T1 PRL and long-T1 PRL volumes and other brain volumetric measures with clinical scales are reported in Figure S6 and Data S1.

PRL, short-T1 PRL, and long-T1 PRL categories were calculated based on the 75th percentile distribution at 4 PRL, 2 short-T1 PRL, and 1 long-T1 PRL, respectively to ensure coherent patient stratification. Twenty-eight patients had at least 4 PRL (27.2%), 37 at least 1 long-T1 PRL (35.9%), and 36 at least 2 short-T1 PRL (35%).

In univariate analysis, patients with ≥1 long-T1 PRL had reduced normalized thalamic volume, higher T2 lesion, and increased normalized choroid plexus (CP) volume (Table 1). No difference in total PRL volume and total short-T1 PRL volume was observed between RRMS and PMS patients ($P/P_{FDR} = 0.35/0.364$ and $P/$

P_{FDR} = 0.209/0.28). Instead, PMS patients had significantly higher volume of long-T1 PRL compared to RRMS patients (386.01 vs. 204.20 mm^3, P/P_{FDR} = 0.004/0,005).

In linear regression analysis, long-T1 PRL volume yielded a higher adjusted R^2 (adj. R^2) than PRL volume (0.074 vs. 0.031), indicating a better fit to the data in terms of explaining the variation in the outcome variable. Both total PRL ($\beta = 3.6 \times 10^{-4}$, 95% CI [$1.4 \times 10^{-5}$, 7.1×10^{-4}], P/P_{FDR} = 0.042/0.057) and total long-T1 PRL ($\beta = 7.8 \times 10^{-4}$, 95% CI [$2.7 \times 10^{-4}$, 1.3×10^{-3}], P/P_{FDR} = 0.003/0.005) volumes were associated with a higher patient's EDSS (dependent variable), although statistical significance for the PRL volume association was lost after FDR correction. However, no statistically significant association between short-T1 PRL volumes and EDSS was found (P/P_{FDR} = 0.8/0.95). Regarding disease severity, both PRL ($\beta = 6.2 \times 10^{-4}$, 95% CI [$2.0 \times 10^{-4}$, 1.1×10^{-3}], P/P_{FDR} = 0.004/0.007) and long-T1 PRL ($\beta = 1.1 \times 10^{-3}$, 95 CI [$4.9 \times 10^{-4}$, 1.8×10^{-3}], P/P_{FDR} = 0.0006/0.001) volumes were significantly associated with MSSS. However, long-T1 PRL volumes showed again better fit for explaining MSSS compared to PRL volumes alone (adj. R^2 = 0.102 vs. 0.069). Representative examples are reported in Figure 4. When correcting for the presence of a recent clinico-radiological relapse within the last 3 months (covariate), the association of PRL and long-T1 PRL volumes with the clinical outcomes did not change (Table S2). Similarly, when adding patient age (Figure S7) as an additional covariate to the EDSS regression analysis, long-T1 PRL volume still yielded a higher adj. R^2 than PRL volume (0.248 vs. 0.208; Table S2), although the difference between the two R^2 appeared clearly reduced when patient age was included in the model.

The random forest analysis, using EDSS or MSSS as outcome variables with PRL and long-T1 PRL volumes as predictors, showed total long-T1 PRL volumes yielded 2.3 times higher importance in explaining EDSS than total PRL volumes (Fig. 5A). Similarly, long-T1 PRL volumes showed 4.2 times higher importance in predicting MSSS compared to PRL volumes (Fig. 5B).

The same random forest analysis using EDSS as outcome variable and categorized PRL (0–3 vs. ≥4 PRL) and long-T1 PRL (0 vs. ≥1 long-T1 PRL) as predictors, showed 1.6 times higher importance for the presence of ≥1 long-T1 PRL than presence of ≥4 PRL (Fig. 5C). This became even more true when using disease severity as the outcome variable: long-T1 PRL versus PRL showed a 9.7 times higher importance in predicting MSSS (Fig. 5D).

Simple linear regression showed that presence of ≥4 PRL was associated with a higher MSSS (β_{add} = 1.38, 95% CI [0.28–2.48], adj. R^2 = 0.048, P/P_{FDR} = 0.015/0.021) compared to <3 PRL. Presence of a single long-T1 PRL was also associated with higher MSSS but yielding twice the predictive strength in explaining the variance of the dependent variable compared to the classical PRL categorization (β_{add} = 1.84, 95% CI [0.85–2.82], adj. R^2 = 0.111, P/P_{FDR} < 0.001). No association with the presence of at least two short-T1 PRL and MSSS was found (adj. R^2 = 0.017, P/P_{FDR} = 0.1). Further analysis is shown in Data S1.

Clinical associations in the MPRAGE cohort

To replicate our results in an extended cohort, using the more clinically available MPRAGE sequence, we included 54 additional patients from Lausanne, as well as 10 additional patients from Brussels for which T1 maps were corrupted but MPRAGE available (see also Fig. 1). This "MPRAGE cohort" thus included a total of 167 patients (Table 2).

Cutoff for categorizing patients based on the number of PRL and long-T1 PRL were again calculated based on the data distribution and were 3 and 1, respectively. The random forest analysis using EDSS as outcome variable revealed 2.1 times higher importance of ≥1 long-T1 PRL compared to ≥3 PRL (Fig. 5E). When using MSSS as outcome variable, ≥1 long-T1 PRL showed 1.4 times higher importance (vs. ≥3 PRL; Fig. 5F). Two regression analyses were conducted using EDSS as dependent variable and PRL or long-T1 PRL categorized patients as independent predictors. Simple linear regression analysis showed that EDSS was on average 0.8 points higher in patients with ≥3 PRL versus <3 (β_{add} = 0.8, 95% CI [0.12–1.45], P/P_{FDR} = 0.022/0.05, R^2 = 0.025). Long-T1 PRL showed, in line with results obtained in the T1 mapping cohort, a higher adjusted R^2 (0.054 vs. 0.025) than classical PRL, with patients having at least one long-T1 PRL showing 1.08 points higher EDSS (β_{add} = 1.08, 95% CI [0.42–1.7], P/P_{FDR} = 0.001/0.003). In line with the EDSS results, PRL and long-T1 PRL were both significantly associated with MSSS. Patients bearing ≥3 PRL had at least 1.57 points higher EDSS (β_{add} = 1.57, 95% CI [0.73–2.4], P/P_{FDR} < 0.001, adjusted R^2 = 0.071), while patients bearing ≥1 long-T1 PRL presented 1.64 points higher MSSS (β_{add} = 1.64, 95% CI [0.83–2.44], P/P_{FDR} < 0.0001/0.001, adjusted R^2 = 0.084). Predictive strength of explaining MSSS variance was again higher for long-T1 PRL. When correcting regression models for center or scanner, no difference in either result was observed (Table S2).

Discussion

In recent years, CAL imaging biomarkers, including PRL, have been proposed as a novel biomarker of MS disease severity and prognosis.[25,29] Imaging studies have shown

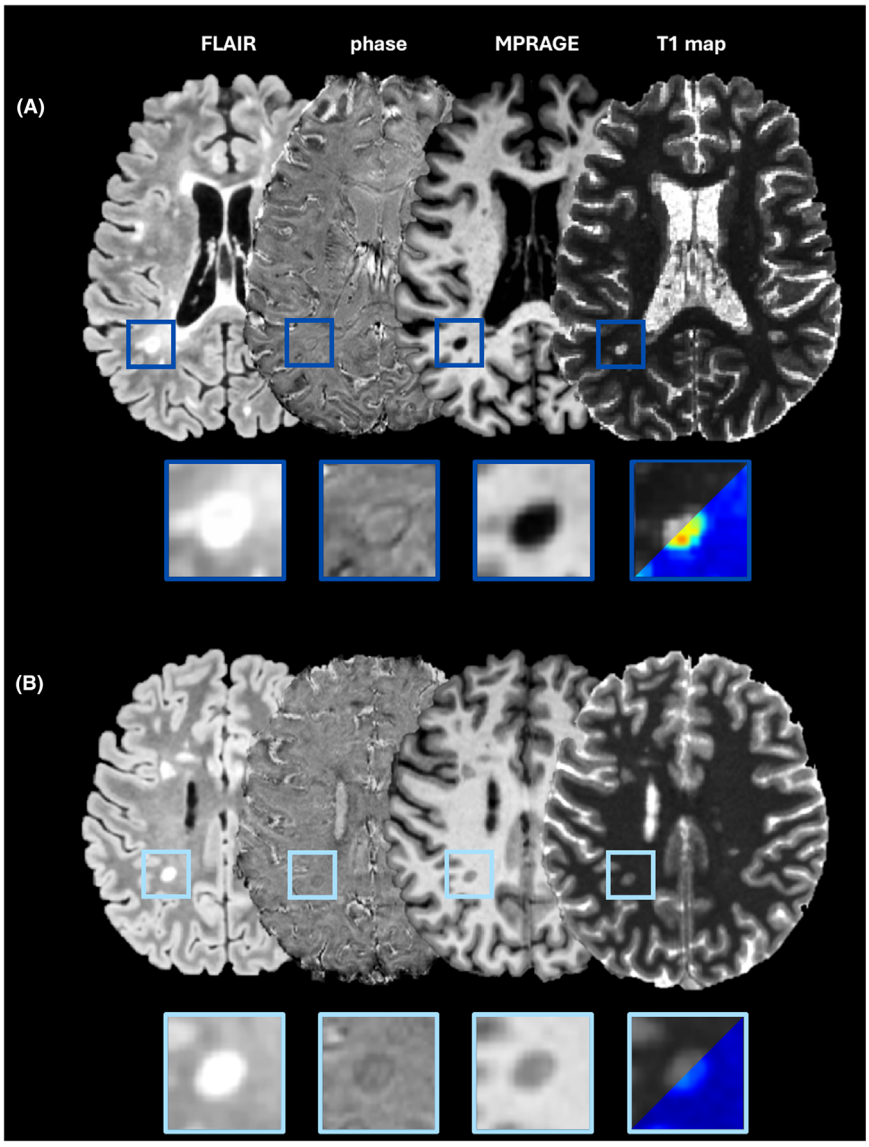

Figure 4. The importance of long-T1 PRL in clinical and MRI metrics. (A) MR images of a 24-year-old RRMS male patient with EDSS of 6 and MSSS of 9.46. The majority of PRL show long-T1 values (dark blue boxes). (B) MR images of a 26-year-old RRMS female patient with EDSS of 2 and MSSS of 5.58. Based on the calculated T1 cutoff, all the detected PRL are considered short-T1 PRL. EDSS, Expanded Disability Status Scale; MSSS, Multiple Sclerosis Severity Score; PRL, paramagnetic rim lesions; RRMS, relapsing–remitting MS.

substantial heterogeneity in terms of PRL-associated tissue damage[6,12,17]; however, its clinical significance is mostly unknown. Here we show that PRL heterogeneity plays a role in the clinical assessment of MS patients.

The key findings of this research can be summarized as follows: (1) there exists significant heterogeneity within PRL – especially regarding microstructural damage within the lesion, which seems associated with (2) the age of a lesion; (3) PRL stratification using T1 mapping and susceptibility-based MRI allow to identify long-T1 highly destructive PRL, which improved overall cross-sectional association with MS clinical scales when compared to short-T1 non-destructive PRL or PRL whatsoever; (4) similar results can be obtained by combining susceptibility-based MRI with more clinically available MRI techniques such as T1-weighted MPRAGE.

MS lesion heterogeneity can be characterized in vivo using quantitative imaging techniques sensitive to both myelin[15,30] and neuroaxonal[12,13,17] damage. In this study, we combined a quantitative estimation of lesional tissue microstructure with susceptibility-based MRI and differentiated non-destructive from highly destructive lesions

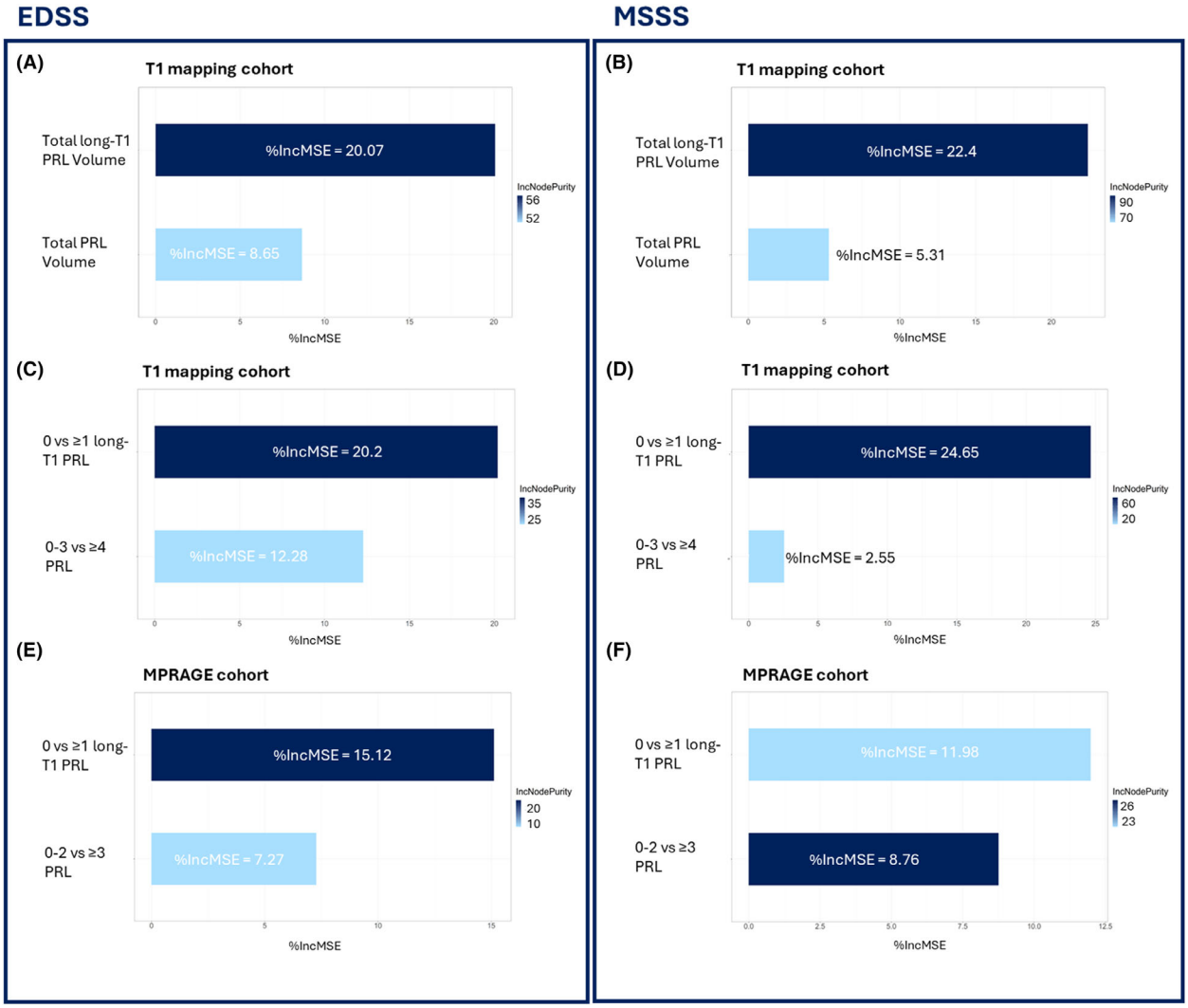

Figure 5. Random forest analysis of clinical metrics. (A) EDSS and (B) MSSS random forest analyses in the T1 mapping cohort using total PRL and total long-T1 PRL volumes as predictors. (C) EDSS and (D) MSSS random forest analyses in the T1 mapping cohort with classic PRL categorization (0–3, ≥4 PRL) and long-T1 PRL categorization (0, ≥1 long-T1 PRL) as predictors. (E) EDSS and (F) MSSS random forest analyses in the MPRAGE cohort with PRL categorization (0–2, ≥3 PRL) and long-T1 PRL categorization (0, ≥1 long-T1 PRL) as predictors.

based on a calculated long-T1 cutoff. We found that long-T1 PRL were significantly older than short-T1 PRL and showed more axonal and myelin damage as respectively suggested by their lower NDI and longer T1 times. In agreement with these findings, we observed a slight increase of lesional T1 over time and patient's age in PRL compared to non-PRL. Looking more in depth to our PRL heterogeneity characterization, in agreement with recent findings on early quantitative susceptibility changes within PRL,[19] we observed that short-T1 PRL featured a T1 increase over time when compared to long-T1 PRL, suggesting that the observed T1 increase in PRL is likely due to tissue damage (i.e., axonal loss) which occurs during the first years of PRL development. This dynamic T1 increase seems to slow down later on, possibly reflecting a gradual reduction of the chronic inflammatory process and of the accompanying tissue damage and, less likely,[31] ongoing remyelination.

Although a large heterogeneity in the visibility of CAL's paramagnetic rims have already been reported,[11,19,32] less is known regarding the relationship between rim visibility and PRL associated tissue damage. In this study we observed a clear association between lesional T1 times and rim visibility; however, we also found that the evolution of rim visibility over time does not seem to follow the same dynamic observed for the average lesional T1. Indeed, our VCLS 5 lesions were not found to be significantly older than VCLS 4 lesions and lesional VCLS was

Table 2. Clinical and MRI demographics of the MPRAGE cohort.

	Long-T1 PRL categorization			Center		
Characteristic	0 long-T1 PRL $N = 106$[a]	≥1 long-T1 PRL $N = 61$[a]	P/P_{FDR}[b]	Brussels $N = 113$[a]	Lausanne $N = 54$[a]	P/P_{FDR}[b]
Age	45.77 (12.19)	44.37 (12.69)	0.4/0.5	43.83 (12.87)	48.24 (10.72)	**0.031/0.044**
Sex						
Male	35/106 (33%)	26/61 (43%)	0.2/0.2	41/113 (36%)	20/54 (37%)	>0.9
Female	71/106 (67%)	35/61 (57%)		72/113 (64%)	34/54 (63%)	
Phenotype						
RRMS	81/106 (76%)	34/61 (56%)	**0.005/0.008**	80/113 (71%)	35/54 (65%)	0.4/0.5
PMS	25/106 (24%)	27/61 (44%)		33/113 (29%)	19/54 (35%)	
Disease duration	10.09 (9.55)	8.67 (9.18)	0.3/0.4	8.99 (9.57)	10.80 (9.04)	0.058/0.078
Treatment at baseline						
Untreated	46/103 (45%)	27/59 (46%)	>0.9	61/113 (54%)	12/49 (24%)	**0.004/0.006**
Platform	8/103 (7.8%)	4/59 (6.8%)		8/113 (7.1%)	4/49 (8.2%)	
High efficacy	34/103 (33%)	18/59 (31%)		29/113 (26%)	23/49 (47%)	
Very high efficacy	15/103 (15%)	10/59 (17%)		15/113 (13%)	10/49 (20%)	
EDSS	2.63 (1.95)	3.70 (2.28)	**0.007/0.01**	2.88 (2.07)	3.31 (2.26)	0.5 /0.5
MSSS	4.14 (2.52)	5.77 (2.56)	**<0.001**	4.64 (2.58)	4.92 (2.80)	0.7/0.8

Bold *P*-values indicate statistical significance ($P < 0.05$). Treatments: platform = injectable platform drugs; high efficacy = teriflunomide, dimethyl fumarate, fingolimod, siponimod, and ozanimod; very high efficacy = ocrelizumab, ofatumumab, rituximab, natalizumab, and cyclophosphamide. CP, choroid plexus; EDSS, Expanded Disability Status Scale; MS, multiple sclerosis; MSSS, Multiple Sclerosis Severity Score; lT1-PRL, long-T1 paramagnetic rim lesion; PMS, primary or secondary progressive MS; PRL, paramagnetic rim lesion; RRMS, relapsing–remitting MS normalized volumes, total structure volume/intracranial volume.

[a]Mean (SD); *n*/*N* (%).

[b]Wilcoxon rank sum test; Pearson's chi-squared test; Fisher's exact test.

found to decrease with increasing patient's age, suggesting, in agreement with existing evidence,[11] an overall decrease in rim visibility over time.

We observed substantial heterogeneity not only regarding the microstructural damage recorded within PRL but also regarding their volume. Indeed, long-T1 PRL were found to be significantly larger than short-T1 PRL, suggesting a possible increase in lesional volume during the early phases of PRL development. It is possible that this volume heterogeneity might help to interpret the limited correspondence reported between PRL and SEL.[10,33] Besides, for what concerns the physiopathology of PRL, our random forest analysis showed that lesional damage (average lesional T1) is more important than lesional volume when differentiating PRL versus non-PRL (Data S1).

In MS, PRL have been associated with worse clinical disability and severity and, most recently, also with progression independent of relapse activity.[3,5] In our study, this previously described association between PRL and clinical outcomes was mainly driven by the presence of highly destructive or long-T1 PRL. Indeed, whether using the number or the volume of these highly destructive lesions, long-T1 PRL better predicted EDSS and MSSS when compared to short-T1 PRL or PRL whatsoever. Additionally, no differences in EDSS or MSSS could be observed between patients having only short-T1 PRL and no PRL. Interestingly, when correcting the association between EDSS and PRL metrics by patient's age, the difference in predictive strength between high-T1 PRL and PRL appeared attenuated; future longitudinal studies should test if other PRL subtypes (like younger short-T1 PRL) may be more suited to predict future disease progression in younger patients. In line with these results, patients with long-T1 PRL showed an overall increased T2 lesion load and cortical lesion burden, reduced thalamic volumes, and enlarged choroid plexus, highlighting the link between these highly destructive PRL and chronic neuroinflammatory and neuroaxonal damage in MS.[34]

One clear limitation of applying this lesion heterogeneity characterization in larger, multicenter clinical studies is the need for quantitative research MRI techniques such as T1 mapping, allowing to estimate the microstructure of lesions. In this study, we show that a similar lesion heterogeneity characterization can be achieved by combining susceptibility-based imaging with more clinically available MRI techniques such as the T1-weighted MPRAGE. Results obtained in the validation MPRAGE cohort were in line with those obtained in the T1 mapping cohort suggesting that lesional T1 intensity cutoff values calculated on the NAWM-normalized MPRAGE represent a relatively simple and fast method to obtain information on tissue integrity, which could be easily implemented in a clinical setting.

The major limitation of this study is the pure cross-sectional nature of the MS clinical outcomes analysis. In addition, study participants in this study received various disease-modifying treatments, and while there were no clear differences in terms of lesion categories among treatment groups, the limited number of participants and the mostly cross-sectional nature of the data here presented makes it challenging to ascertain whether disease-modifying treatments may influence the volume and/or T1 of either short- or long-T1 PRL. Moreover, the sample size of the age-tracked lesions was relatively small and we could not study the potential effect of treatment and of disease phenotype in our longitudinal lesion age analysis.

We believe that prospective studies are needed to investigate the predictive value of heterogeneous PRL on disability progression as well as the effect of MS disease-modifying treatments on these heterogeneous lesions. Indeed, previous evidence suggests only a limited treatment effects on CAL's quantitative T1, magnetic susceptibility, or volume.[5,35,36] Following the findings reported here, future studies should take CAL's heterogeneity into account and focus on the effect of MS drugs on PRL which are still in their early developmental stage (short-T1 PRL) and might therefore be more susceptible to the effect of disease-modifying treatments. Finally, comparative MRI-histopathological studies should investigate whether different subpopulations of pro-inflammatory cells can be found during the development of PRL, reflecting the accelerated process of axonal and myelin damage recorded early during the development of PRL.

In conclusion, PRL are heterogeneous in terms of lesional T1, volume, and rim visibility. Average lesional T1 time seems to be linked to the age of a lesion and younger, short-T1 PRL show accelerated tissue damage accumulation compared to older, long-T1 PRL. Long-T1 PRL seems to cross-sectionally improve the prediction of MS clinical outcomes, suggesting the importance of characterizing PRL heterogeneity in future physiopathological and clinical studies.

Overall, these findings are based on a relatively small lesion and patient dataset and need to be confirmed in larger MS cohorts.

Acknowledgments

The authors thank the study participants; the neuroimmunology clinic of Cliniques Universitaires Saint-Luc for recruiting and evaluating the participants and for coordinating the scans; Martina Absinta (IRCCS San Raffaele Scientific Institute) for helping with data analysis and interpretation; Pascal Sati (Cedars-Sinai Medical Center), Francesco La Rosa (Icahn School of Medicine at Mount Sinai), Meritxell Bach Cuadra (University of Lausanne), Pedro M Gordaliza (University of Lausanne), Francois Guisset (Université catholique de Louvain), Océane Perdaens (Université catholique de Louvain), Laurence Dricot (Université catholique de Louvain), and Julie Poujol (GE Healthcare) for assistance with 3T MRI scan acquisition and analysis.

Author Contributions

Anna Stölting: writing – review and editing, writing – original draft, visualization, validation, methodology, investigation, formal analysis, data curation, and conceptualization. Colin Vanden Bulcke, Serena Borrelli, and Céline Bugli: writing – review and editing, writing – original draft, formal analysis, and data curation. Renaud Du Pasquier: writing – review and editing, writing – original draft, and supervision. Vincent van Pesch: writing – review and editing, writing – original draft, and data curation. Pietro Maggi: writing – review and editing, writing – original draft, supervision, investigation, and conceptualization.

Funding Information

Anna Stölting has the financial support of the Fédération Wallonie Bruxelles – Fonds Spéciaux de Recherche (F.S.R), Université catholique de Louvain. Colin Vanden Bulcke has the financial support of the Fonds de Recherche Clinique (FRC), Université catholique de Louvain. Serena Borrelli is supported by the Funds Claire Fauconnier, Ginette Kryksztein & José, and Marie Philippart-Hoffelt managed by the King Baudouin Foundation. Pietro Maggi's research activity is supported by the Fondation Charcot Stichting Research Fund 2023, the Fund for Scientific Research (F.R.S, FNRS; grant no. 40008331), Cliniques universitaires Saint-Luc "Fonds de Recherche Clinique," and Biogen.

Conflict of Interest

Anna Stölting, Colin Vanden Bulcke, Céline Bugli and Renaud du Pasquier have nothing to declare. Serena Borrelli received unrelated research funding from Roche, Sanofi, and Brugmann Foundation and speaker/consulting honoraria from Sanofi, Roche, Janssen, Merck, and Novartis. Vincent van Pesch received travel grants from Merck Healthcare kGaA (Darmstadt, Germany), Biogen, Sanofi, Bristol Meyer Squibb, Almirall, and Roche. His institution has received research grants and consultancy fees from Roche, Biogen, Sanofi, Merck Healthcare kGaA (Darmstadt, Germany), Bristol Meyer Squibb, Janssen,

Almirall, Novartis Pharma, and Alexion. Pietro Maggi's research activity is supported by the Fondation Charcot Stichting Research Fund 2023, the Fund for Scientific Research (F.R.S, FNRS; grant no. 40008331), Cliniques universitaires Saint-Luc "Fonds de Recherche Clinique," and Biogen. Received consulting honoraria from Sanofi, Biogen, and Merck.

Data Availability Statement

The data that support the findings of this study are controlled by the respective centers and are not publicly available. Request to access the anonymized individual patient data should be forwarded to data controllers via the corresponding author. Written requests for access to the derived data will be considered by the corresponding author and a decision made about the appropriateness of the use of the data.

References

1. Giovannoni G, Popescu V, Wuerfel J, et al. Smouldering multiple sclerosis: the 'real MS'. Ther Adv Neurol Disord. 2022;15:17562864211066751.
2. Müller J, Cagol A, Lorscheider J, et al. Harmonizing definitions for progression independent of relapse activity in multiple sclerosis: a systematic review. JAMA Neurol. 2023;80:1232-1245.
3. Absinta M, Sati P, Masuzzo F, et al. Association of chronic active multiple sclerosis lesions with Disability in vivo. JAMA Neurol. 2019;76:1474-1483.
4. Cagol A, Benkert P, Melie-Garcia L, et al. Association of spinal cord atrophy and brain paramagnetic rim lesions with progression independent of relapse activity in people with MS. Neurology. 2024;102:e207768.
5. Maggi P, Bulcke CV, Pedrini E, et al. B cell depletion therapy does not resolve chronic active multiple sclerosis lesions. EBioMedicine. 2023;94:104701.
6. Kuhlmann T, Ludwin S, Prat A, Antel J, Brück W, Lassmann H. An updated histological classification system for multiple sclerosis lesions. Acta Neuropathol. 2017;133:13-24.
7. Kuhlmann T, Klotz L, Smolders J, Huitinga I. Rapid MS disease progression is histopathologically associated with a new lesions type. In ECTRIMS 2022 LB Poster, Multiple Sclerosis Journal (Amsterdam, 2022). Vol 28:956-983. doi:10.1177/13524585221126909
8. Kaunzner UW, Kang Y, Zhang S, et al. Quantitative susceptibility mapping identifies inflammation in a subset of chronic multiple sclerosis lesions. Brain J Neurol. 2019;142:133-145.
9. Absinta M, Sati P, Schindler M, et al. Persistent 7-tesla phase rim predicts poor outcome in new multiple sclerosis patient lesions. J Clin Invest. 2016;126:2597-2609.
10. Dal-Bianco A, Grabner G, Kronnerwetter C, et al. Slow expansion of multiple sclerosis iron rim lesions: pathology and 7 T magnetic resonance imaging. Acta Neuropathol. 2017;133:25-42.
11. Dal-Bianco A, Grabner G, Kronnerwetter C, et al. Long-term evolution of multiple sclerosis iron rim lesions in 7 T MRI. Brain. 2021;144:833-847.
12. Vanden Bulcke C, Stölting A, Maric D, Macq B, Absinta M, Maggi P. Comparative overview of multi-shell diffusion MRI models to characterize the microstructure of multiple sclerosis lesions and periplaques. NeuroImage Clin. 2024;42:103593.
13. Rahmanzadeh R, Lu PJ, Barakovic M, et al. Myelin and axon pathology in multiple sclerosis assessed by myelin water and multi-shell diffusion imaging. Brain J Neurol. 2021;144:1684-1696.
14. Krajnc N, Schmidbauer V, Leinkauf J, et al. Paramagnetic rim lesions lead to pronounced diffuse periplaque white matter damage in multiple sclerosis. Mult Scler J. 2023;29:1406-1417.
15. Kolb H, Absinta M, Beck ES, et al. 7T MRI differentiates remyelinated from demyelinated multiple sclerosis lesions. Ann Neurol. 2021;90:612-626.
16. Absinta M, Sati P, Gaitán MI, et al. Seven-tesla phase imaging of acute multiple sclerosis lesions: a new window into the inflammatory process. Ann Neurol. 2013;74:669-678.
17. Rahmanzadeh R, Galbusera R, Lu PJ, et al. A new advanced MRI biomarker for remyelinated lesions in multiple sclerosis. Ann Neurol. 2022;92:486-502.
18. Weber CE, Wittayer M, Kraemer M, et al. Long-term dynamics of multiple sclerosis iron rim lesions. Mult Scler Relat Disord. 2022;57:103340.
19. Zhang S, Nguyen TD, Rúa SH, et al. Quantitative susceptibility mapping of time-dependent susceptibility changes in multiple sclerosis lesions. AJNR Am J Neuroradiol. 2019;40:987-993.
20. Thaler C, Faizy T, Sedlacik J, et al. T1- thresholds in black holes increase clinical-radiological correlation in multiple sclerosis patients. PLoS One. 2015;10:e0144693.
21. Kurtzke JF. Rating neurologic impairment in multiple sclerosis: an expanded disability status scale (EDSS). Neurology. 1983;33:1444-1452.
22. Roxburgh RHSR, Seaman SR, Masterman T, et al. Multiple sclerosis severity score: using disability and disease duration to rate disease severity. Neurology. 2005;64:1144-1151.
23. Thompson AJ, Banwell BL, Barkhof F, et al. Diagnosis of multiple sclerosis: 2017 revisions of the McDonald criteria. Lancet Neurol. 2018;17:162-173.
24. Fischl B, Salat DH, Busa E, et al. Whole brain segmentation: automated labeling of neuroanatomical structures in the human brain. Neuron. 2002;33:341-355.
25. Bagnato F, Sati P, Hemond CC, et al. Imaging chronic active lesions in multiple sclerosis: a consensus statement. Brain. 2024;147:2913-2933. doi:10.1093/brain/awae013

26. Zhang H, Schneider T, Wheeler-Kingshott CA, Alexander DC. NODDI: practical in vivo neurite orientation dispersion and density imaging of the human brain. NeuroImage. 2012;61:1000-1016.
27. R Core Team. R: a language and environment for statistical computing. R Foundation for Statistical Computing. (2023).
28. Liaw, A. & Wiener, M. Classification and regression by randomForest. R News. (2002).
29. Borrelli S, Martire MS, Stölting A, et al. Central vein sign, cortical lesions, and paramagnetic rim lesions for the diagnostic and prognostic workup of multiple sclerosis. Neurol Neuroimmunol Neuroinflamm. 2024;11:e200253.
30. Maggi P, Macri SMC, Gaitán MI, et al. The formation of inflammatory demyelinated lesions in cerebral white matter. Ann Neurol. 2014;76:594-608.
31. Chang A, Tourtellotte WW, Rudick R, Trapp BD. Premyelinating oligodendrocytes in chronic lesions of multiple sclerosis. N Engl J Med. 2002;346:165-173.
32. Absinta M, Sati P, Reich DS. Advanced MRI and staging of multiple sclerosis lesions. Nat Rev Neurol. 2016;12:358-368.
33. Calvi A, Haider L, Prados F, Tur C, Chard D, Barkhof F. In vivo imaging of chronic active lesions in multiple sclerosis. Mult Scler. 2022;28:683-690.
34. Fleischer V, Gonzalez-Escamilla G, Ciolac D, et al. Translational value of choroid plexus imaging for tracking neuroinflammation in mice and humans. Proc Natl Acad Sci USA. 2021;118:e2025000118.
35. Zinger N, Ponath G, Sweeney E, et al. Dimethyl fumarate reduces inflammation in chronic active multiple sclerosis lesions. Neurol Neuroimmunol Neuroinflamm. 2022;9:e1138.
36. Elliott C, Belachew S, Wolinsky JS, et al. Chronic white matter lesion activity predicts clinical progression in primary progressive multiple sclerosis. Brain J Neurol. 2019;142:2787-2799.

Supporting Information

Additional supporting information may be found online in the Supporting Information section at the end of the article.

Data S1. Supplementary material and methods.
Figure S1. Scatter plot of normalized MPRAGE intensity values and T1 map derived T1 values based on visual confidence level score.
Figure S2. PRL normalized T1 intensity values in Brussels (violet) and Lausanne (green).
Figure S3. Visualization of mixed model analysis with random subject effect of T1 increase in PRL and non-PRL over the patient's age.
Figure S4. Distribution of T1 times in the 3 groups of qualitatively rated lesion. Red dotted line indicates the calculated quantitative long-T1 cutoff.
Figure S5. Visualization of repeated measures mixed model analysis with random subject and lesion effect of T1 evolution over follow up time in short-T1 and long-T1 PRL.
Figure S6. Spearman correlations of different lesion metrics with clinical and brain volumetric measures.
Figure S7. Volume distribution of short-T1 and long-T1 PRL over the patients' age.
Table S1. Multiple sclerosis lesion characteristics.
Table S2. Additional regression models.

